



Experimental investigation of soot morphological transformation and its impact on size-resolved light absorption

Joel Kuula^{1,2}, Juho Karhu¹, Tommi Mikkonen¹, Aki Virkkula², Hilkka Timonen², Tuomas Hieta¹, Markku Vainio^{1,3}

- ¹Department of Chemistry, University of Helsinki, Helsinki, FI-00560, Finland
 - ²Atmospheric Composition Research, Finnish Meteorological Institute, Helsinki, FI-00560, Finland
 - ³Photonics Laboratory, Physics Unit, Tampere University, Tampere, FI-33100, Finland

Correspondence to: Joel Kuula (joel.kuula@helsinki.fi)

Abstract. This study experimentally investigated the influence of aggregate morphology on soot light absorption. Fresh soot was generated using an inverted-flame burner and compacted through controlled humidification—drying cycles to isolate the effects of structural transformation from those of chemical composition or coating. Size-resolved absorption measurements were performed at three wavelengths (440, 516, and 635 nm) using a cantilever-enhanced photoacoustic spectrometer (CEPAS) coupled with a differential mobility analyzer (DMA) and a centrifugal particle mass analyzer (CPMA). For small particles, the absorption cross-section increased after compaction but decreased for larger particles, with the wet-to-dry absorption ratio transitioning from values above unity to below unity as particle mass increased. The tipping point occurred in the 1–2 fg mass range, corresponding to a volume-equivalent diameter of approximately 102–129 nm for spherical particles at a soot material density of 1.8 g cm⁻³. This behavior suggests a competition between near-field dipole—dipole coupling, which enhances optical absorption in moderately compact aggregates, and optical shielding, which suppresses absorption in highly compact structures. The findings are consistent with theoretical predictions and numerical studies of aggregate optics, providing experimental evidence for morphology-dependent absorption transitions. These results emphasize the importance of accurately representing soot morphology in optical and climate models and motivate further controlled experiments to disentangle the effects of structure, coating, and composition on soot radiative properties.

1 Introduction

Freshly emitted soot, a byproduct of incomplete combustion, forms chain-like aggregates composed of nanometer-sized spherules or monomers (Michelsen, 2017; Sorensen, 2011; Wentzel et al., 2003). These aggregates exhibit a fractal-like structure, with their optical and physical properties governed by their fractal dimension and the arrangement of individual monomers (Bescond et al., 2013; Brasil et al., 1999). Once emitted into the atmosphere, soot undergoes various aging processes such as condensation of secondary species, coagulation, and exposure to varying humidity levels (Khalizov et al., 2009; Pagels et al., 2009; Zhang et al., 2008). These processes drive morphological transformations, typically compacting the soot aggregates from open, lacy structures into smaller, near-spherical forms (Adachi et al., 2010; China et al., 2013,

https://doi.org/10.5194/ar-2025-38

Preprint. Discussion started: 24 November 2025

© Author(s) 2025. CC BY 4.0 License.



35

50



2015). Such restructuring often coincides with particle growth and coating formation, both of which modify the way soot interacts with radiation (Cappa et al., 2019; Liu et al., 2017; Matsui et al., 2018).

The consequences of these transformations on optical properties are commonly described in terms of light absorption enhancement, also known as the lensing effect, where the absorption cross-section of aged soot exceeds that of fresh soot (Cappa et al., 2012; Lack et al., 2009). This enhancement is driven by multiple concurrent mechanisms, including refractive focusing by non-absorbing coatings, internal multiple scattering, and near-field electromagnetic interactions among monomers (Fuller, 1995; Liu et al., 2008; Scarnato et al., 2013). Absorption enhancement factors ranging from approximately 1 to 3.5 have been reported, depending on the coating thickness, particle morphology, and mixing state (Liu et al., 2017, 2015; Peng et al., 2016; Wu et al., 2018; Zhang et al., 2018).

Despite these advances, the isolated influence of morphology, separated from coating and compositional effects, remains poorly constrained. Numerical and experimental studies have yielded conflicting results: while several works report that aggregate compaction enhances absorption through increased electromagnetic coupling (Dong et al., 2015; Luo et al., 2018; Romshoo et al., 2021; Yon et al., 2015), others find that increasing compactness suppresses absorption due to optical shielding within dense aggregates (Kahnert and Devasthale, 2011; Scarnato et al., 2013). The interplay between these mechanisms appears to depend strongly on particle size, wavelength, and fractal dimension, complicating attempts to generalize morphology–optics relationships (Kahnert and Kanngießer, 2020). Furthermore, most laboratory investigations have focused on coated or internally mixed soot, whereas systematic experiments isolating morphology-driven effects remain scarce.

The present study addresses this gap by experimentally isolating the effect of morphological restructuring on particle size-resolved light absorption. Fresh soot particles were generated using an inverted-flame burner and subsequently compacted through a controlled humidification—drying cycle, mimicking structural evolution during atmospheric aging while avoiding coating effects. Absorption measurements were conducted at three wavelengths using a Cantilever-Enhanced Photoacoustic Spectrometer (CEPAS) (Karhu et al., 2021) coupled with a Differential Mobility Analyzer (DMA) and a Centrifugal Particle Mass Analyzer (CPMA). By combining size-resolved optical data with independent mass and morphology metrics, the goal is to provide quantitative insight into how morphology and particle size jointly affect absorption efficiency, thereby supporting improved parameterizations of soot optical properties in climate and air quality models.

2 Materials and methods

2.1 Instrumentation

An inverted-flame burner (Miniature Inverted Soot Generator, Argonaut Scientific Corp., Canada) operated with a mixture of ethylene gas and compressed air was used to generate fresh soot particles. The flow rates for ethylene and compressed air were 0.081 L min-1 and 9 L min-1, respectively. These flow rates produce an open-tip flame, which generates an abundance of particles; the measured mode of the number size distribution was at ~180 nm and the respective peak concentration was

https://doi.org/10.5194/ar-2025-38 Preprint. Discussion started: 24 November 2025

© Author(s) 2025. CC BY 4.0 License.



75



~2.5 x 104 cm-3 (these particle properties may vary depending on the sampling configuration used, e.g. different dilution rates). Further details on the burner design and its operating regimes can be found in Bischof et al. (2020), Kazemimanesh et al. (2019), and Moallemi et al. (2019), which provide thorough evaluations of operating parameters and resulting particle properties.

A Cantilever-Enhanced Photoacoustic Spectrometer (CEPAS) in conjunction with a Differential Mobility Analyzer (DMA) was used to measure the particle size-resolved light absorption. The main difference between the CEPAS and conventional photoacoustic spectrometers is its detector design. In CEPAS, the detection technique is based on a silicon cantilever whose pressure-induced bending is measured optically using an interferometer. This allows for higher sensitivity (0.013 Mm-1 measured by Karhu et al. 2021) than what is typically achieved using stretching-based membrane microphones found in conventional photoacoustic instruments. In addition, CEPAS also measures the sample only when the detector cell is closed: apart from a separate bypass flow, no continuous flow passes through the CEPAS detector. The sample exchange process is controlled using valves, which periodically divert the sample flow either through the cell or through the bypass line. A single measurement point takes 10 seconds to measure; 5 seconds for cell flushing and sample stabilization and 5 seconds for the measurement itself. Both the bypass and sample flow rates were 0.3 L min-1. The wavelengths used with CEPAS are 440, 516, and 635 nm. A summary of the technical specifications of the CEPAS is shown in Table 1. Moreover, studies by Karhu et al. (2021, 2025) provide comprehensive characterizations for the cantilever-enhanced photoacoustic technique. Although absolute measurement accuracy was not critical in this study, the CEPAS was calibrated using nigrosin reference particles and Mie-modelling prior to conducting experiments. The detailed process and results of the calibration can be found in Kuula et al. (2025).

For the DMA, a long-column (TSI Inc., USA) was used together with aftermarket high-voltage and sheath flow controls to provide additional functionality. The whole DMA-CEPAS system was operated using a custom LabVIEW program. The sheath flow was maintained in a closed-loop arrangement with a manually adjustable blower. Temperature and relative humidity (RH) in the sheath flow loop were monitored with a Sensirion SHT75 sensor (Sensirion AG, Switzerland). Downstream of the DMA, a model 3776 Condensation Particle Counter (CPC, TSI Inc., USA) operated alongside the CEPAS to monitor particle number concentrations. The operating parameters of the DMA are listed in Table 1.





Table 1. CEPAS and DMA key specifications and running parameters. The CEPAS wavelength-specific parameters (e.g. laser power) are listed in the order of blue, green, and red.

Silicon cantilever whose position is measured using interferometer							
Cylindrical; length 90 mm, diameter 4 mm							
440, 516, and 635 nm							
85, 125, and 135 Hz (non-resonant type)							
300, 210, and 130 mW							
Adjustable, min. 10 s							
6 L min ⁻¹							
0.6 L min ⁻¹							
100 nm							
500 nm							
12							
100, 116, 134, 155, 180, 208, 241, 278, 322, 373, 432, and 500 nm							

A Centrifugal Particle Mass Analyzer (CPMA, Cambustion Ltd., UK) was used to measure particle mass. Knowing particle mass, it is possible to derive particle effective density (defined as particle mass divided by the particle electrical mobility diameter-based spherical volume) and hence an approximation of the particle morphological state. Moreover, the mass also enables calculation of a dynamic shape factor, which in this study was used to represent particle morphology numerically (see section 2.3 Data processing). It is worth noting that morphology (shape) affects the particle mobility diameter, and therefore particles passing through the DMA with fixed voltage are not the same if the particle is in fractal form or if it is in a more compact spherical form. That is why the data analysis in this study was carried out as a function of particle mass and not as a function of particle electrical mobility diameter (see section 2.3 Data processing). This approach assumes that particle mass remains unchanged during the humidification—drying process. The CPMA was operated downstream the DMA and prior to the CPC. Each mobility diameter was scanned for peak mass with the scan range adjusted individually for each mobility diameter.

2.2 Sampling and sample treatment

100

A diagram of the sampling configuration is shown in Figure 1. The generated fresh soot particles were first fed through a cyclone to remove larger particles ($Dp > 2.5 \mu m$) from the aerosol stream. However, the collection cup of the cyclone, as



110

115

120

125

130



well as the sample lines downstream of it, were found to be covered in black powdery soot after only a few hours of operation. It was therefore concluded that coagulation-induced particle growth, and thus particle sizes larger than the cyclone cutoff, were likely present in the sample aerosol regardless to some extent. After the cyclone, the sample was diluted in a custom diluter at a ratio of 3:5 (sample flow 3 L min⁻¹, dilution flow 5 L min⁻¹). An analog differential pressure meter was used to measure and adjust the sample aerosol flow entering the diluter. Following dilution, either dry (RH <5%, compressed air) or humidified (RH >95%, a bubbler using de-ionized water) air at a flow rate of 3 L min⁻¹ was introduced to control the sample humidity and restructure soot morphology prior to entry into the Potential Aerosol Mass (PAM) chamber.

The PAM chamber itself is a cylindrical pipe with a diameter of 22 cm and a length of 46 cm (total volume ≈ 13.3 L, corresponding to a sample residence time of approximately 3 min 48 s). Unlike in this study, the PAM chamber is typically used to induce oxidation and photochemical aging of aerosols by applying ultraviolet (UV) irradiance and mixing the sample with volatile organic compounds (VOCs). In the present work, however, the PAM chamber was used solely as a conditioning platform to facilitate future comparisons with more complex aging studies. An additional carrier flow of 4 L min⁻¹ was passed through the PAM. The sample RH was measured immediately downstream of the PAM chamber using a Vaisala HMP60 humidity and temperature probe (Vaisala Oyj, Finland) and subsequently reduced using a silica gel dryer. This step ensured stable and valid CEPAS measurements and minimized any potential optical artifacts caused by residual water on the particles. For clarity in terminology, the term "wet sample" used here and elsewhere specifically refers to a "wet-then-dried" sample; the objective of this study is to isolate only the effect of soot morphological changes. The entire sampling configuration was operated under slight overpressure by restricting the excess flows.

Due to practical limitations (instrument availability and software synchronization), the measurements were conducted in two phases. First, size-resolved light absorption was measured for both wet and dry aerosols. Subsequently, in the second phase, the particle masses were quantified using the CPMA. A typical, single experiment was conducted as follows: the soot generator was started and left to stabilize for 30 mins. After stabilization, the flow rates and the RH levels within the system were checked, and if cleared, the measurement for dry conditions was started. Upon reaching halfway through the day, the humidifier (i.e. bubbler) was switched on and the sample humidity level was left to stabilize. After reaching sufficient humidity level (>90 %) at the PAM chamber, the measurement was continued for the rest of the day. This measurement protocol was the same for both phase 1 and 2.





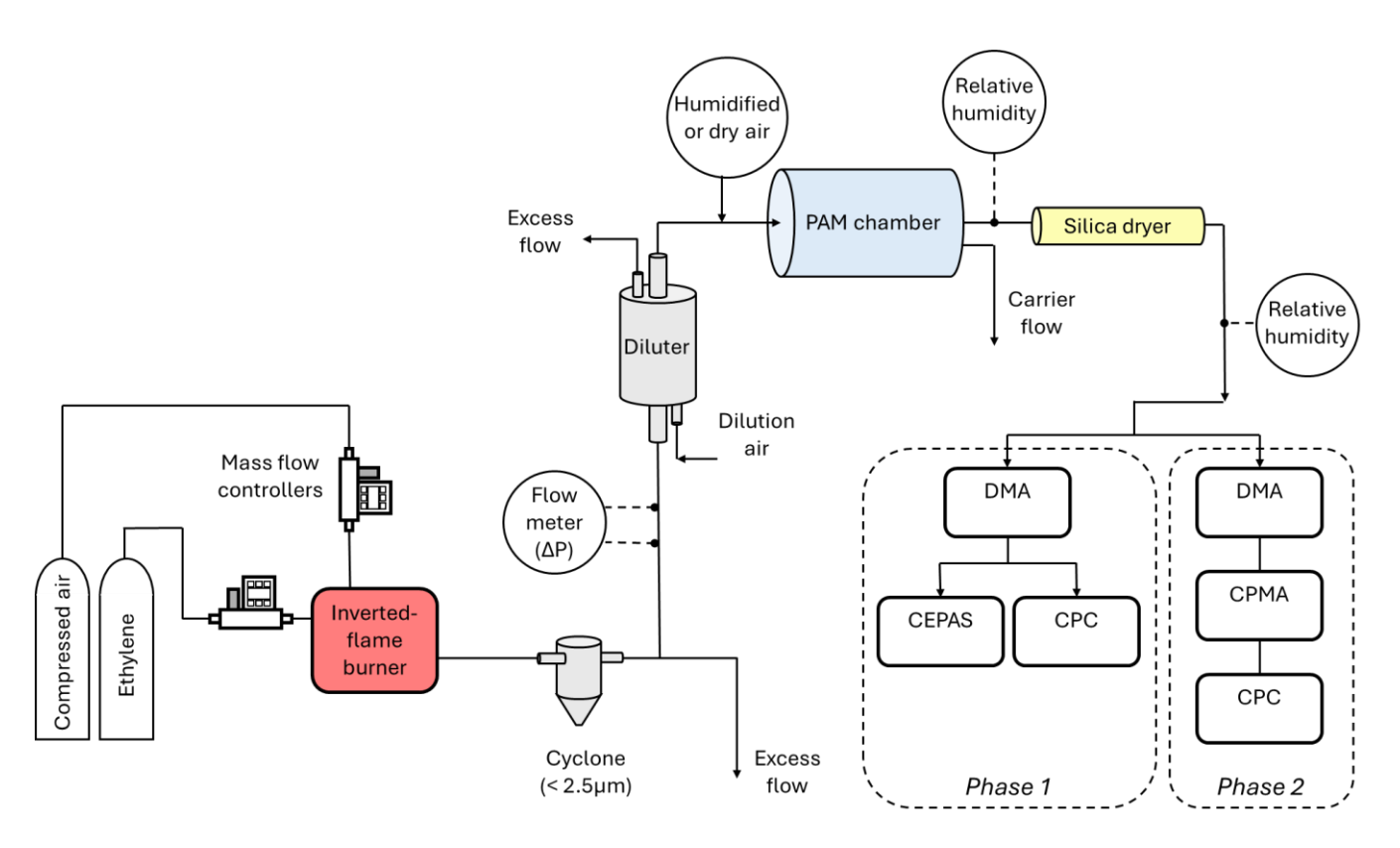


Figure 1. Particle generation setup and sampling configuration in phases 1 and 2.

135 To ensure comparability between the wet and dry aerosol absorption measurements, the absorption was normalized by the particle number concentration to obtain per-particle absorption cross-section (σ). This metric was then used to calculate the wet-to-dry absorption ratio (σ_{wet}/σ_{dry}). Data were filtered to retain only clearly defined wet and dry conditions: measurements with RH > 80% were considered wet, and those with RH < 20% were considered dry. Outliers in the per-particle absorption were removed using the median absolute deviation (MAD) criterion with a factor of 3, meaning that points more than three medians away from the group median were excluded. The MAD is a robust statistic that reduces the influence of single extreme outliers, which can otherwise distort outlier detection when using standard deviation–based methods (Leys et al., 2013). This data processing procedure was applied across all particle sizes and all three CEPAS wavelengths, resulting in a total of 4797 valid data points. For these points, the average RH values for the wet and dry conditions were 95.0 ± 1.6% and 17.3 ± 1.4% (mean ± standard deviation), respectively. The relatively high RH in the dry sample (compared to <5% in compressed air) is due to water vapor produced by the burner combustion process.

Similarly to effective density, the dynamic shape factor (χ) describes the morphology of a particle – and more specifically – the deviation of a particle's aerodynamic or mobility behavior from that of an idealized sphere of the same volume (DeCarlo





et al., 2004). For mobility-based measurements in the transition regime, where slip effects are significant, χ is defined as (Eq. 1):

150

155

170

175

$$\chi = \frac{d_m C_C(d_{ve})}{d_{ve} C_C(d_m)} \tag{1}$$

where d_{ve} is the volume-equivalent diameter (i.e., the diameter of a sphere with the same volume as the particle), d_m is the mobility-equivalent diameter measured by the DMA, and C_c is the Cunningham slip correction factor. The volume-equivalent diameter can be obtained from particle mass (m_p) by assuming spherical geometry and unit density (Eq. 2):

$$d_{ve} = \left(\frac{6m_p}{\pi\rho_0}\right)^{\frac{1}{3}} \tag{2}$$

where ρ_0 is the unit (or material) density of soot (1.8 g cm⁻³ used in this study; Bond and Bergstrom, 2006). The slip correction factor was calculated using the standard Davies (1945) parameterization (Eq. 3):

$$C_c(D_p) = 1 + \frac{2\lambda}{D_p} (1.257 + 0.40e^{-1.1\frac{D_p}{2\lambda}})$$
 (3)

where λ is the mean free path of air under experimental conditions ($\lambda = 66$ nm, corresponding to T = 20°C and p = 1 atm).

For soot which consists of fractal-like agglomerates, χ is significantly larger than unity, reflecting their irregular morphology and increased drag. Upon restructuring at elevated RH, particles become more compact, and χ approaches unity, indicating behavior closer to spherical particles. In this study, χ was calculated for each mobility diameter selected by the DMA using the corresponding peak mass measured with the CPMA. This approach allowed morphology to be quantified consistently across the particle size range and directly related to the measured per-particle absorption.

As noted in the Instrumentation section, all data analysis and presentation in this study were carried out as a function of particle mass rather than electrical mobility diameter. This choice was necessary because morphological differences between wet and dry particles cause the relationship between mobility diameter and particle mass to differ. Consequently, direct comparison of absorption at fixed mobility diameters would not correspond to the same physical particles. To enable a consistent comparison, the measured absorption data were interpolated by fitting suitable functional forms separately for the wet and dry conditions. Different goodness-of-fit criteria, including summed-square error (SSE) and root-mean-square error (RMSE), were evaluated to select the most appropriate fitting functions. The wet-to-dry absorption ratio was then calculated as the pointwise division of the two fitted curves at identical particle masses. The functional forms used for fitting are presented in the figures.





Uncertainty estimation for the per-particle absorption cross-section ratio $\sigma_{wet}/\sigma_{dry}$, which was obtained as the pointwise division of the two fitted curves, was performed by propagating the standard deviations of the fitted σ values. For each particle mass bin, per-particle absorption means and standard deviations were first calculated separately for both dry and wet conditions. The standard deviations of the wet and dry σ were interpolated onto the common mass grid, and standard error propagation was applied, as follows (Eq. 4):

185
$$\Delta \left(\frac{\sigma_{wet}}{\sigma_{dry}}\right) \approx \frac{\sigma_{wet}}{\sigma_{dry}} \sqrt{\left(\frac{\Delta\sigma_{wet}}{\sigma_{wet}}\right)^2 + \left(\frac{\Delta\sigma_{dry}}{\sigma_{dry}}\right)^2}$$
 (4)

where Δ denotes standard deviation.

3 Results and discussion

3.1 Soot morphological transformation

The soot particle effective densities as a function of particle mass for wet and dry particles are shown in Figure 2. For reference, the measured wet and dry particle masses along with their corresponding mobility diameters are also listed in Table 2. In both wet and dry cases, the effective density was highest at the smallest particle sizes and decreased systematically with increasing mass. For wet particles, the effective density decreased from 690 to 173 kg m⁻³, whereas for the dry particles the corresponding decrease was from 579 to 130 kg m⁻³. These values are in an agreement with previous studies reporting fresh soot effective densities (e.g. Leskinen et al., 2023). In relative terms, the wet particles were approximately 21–65% denser across the measured size range, as shown by the dashed black line. Overall, the effective density data indicates that wet particles underwent restructuring and transformed into a more compact morphology.





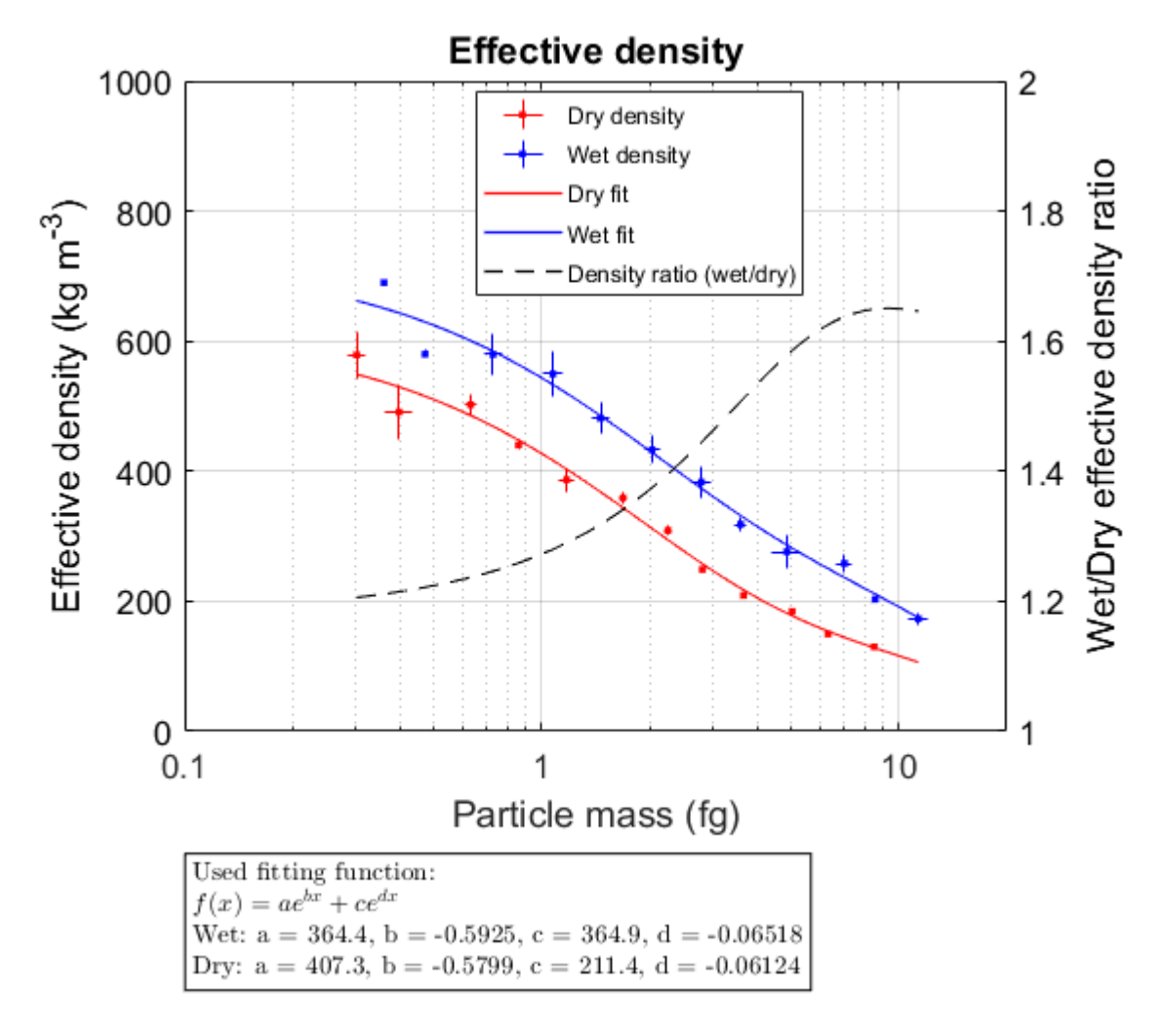


Figure 2. Effective density (mean ± standard deviation) of wet and dry soot particles as a function of particle mass, together with the wet-to-dry effective density ratio.

Table 2. The measured masses of wet and dry particles and their corresponding mobility-diameters.

Mobility diameter (nm)	100	116	134	155	180	208	241	278	322	373	432	500
Wet mass (fg)	0.36	0.47	0.73	1.1	1.5	2.0	2.8	3.6	4.8	7.0	8.6	11
Dry mass (fg)	0.30	0.40	0.63	0.86	1.2	1.7	2.3	2.8	3.7	5.0	6.3	8.5

The effective density trends are consistent with the particle dynamic shape factors (χ), which are shown in Figure 3. As expected, χ increased with particle size for both wet (from 1.8 to 2.9) and dry (from 2.0 to 3.6) conditions, indicating the increasing branching and overall shape complexity with growing mobility diameter and mass. For reference, the often-reported fractal dimension (D_f) of wet and dry particles was 2.16 and 2.06, respectively. The fractal dimension was derived



210

215

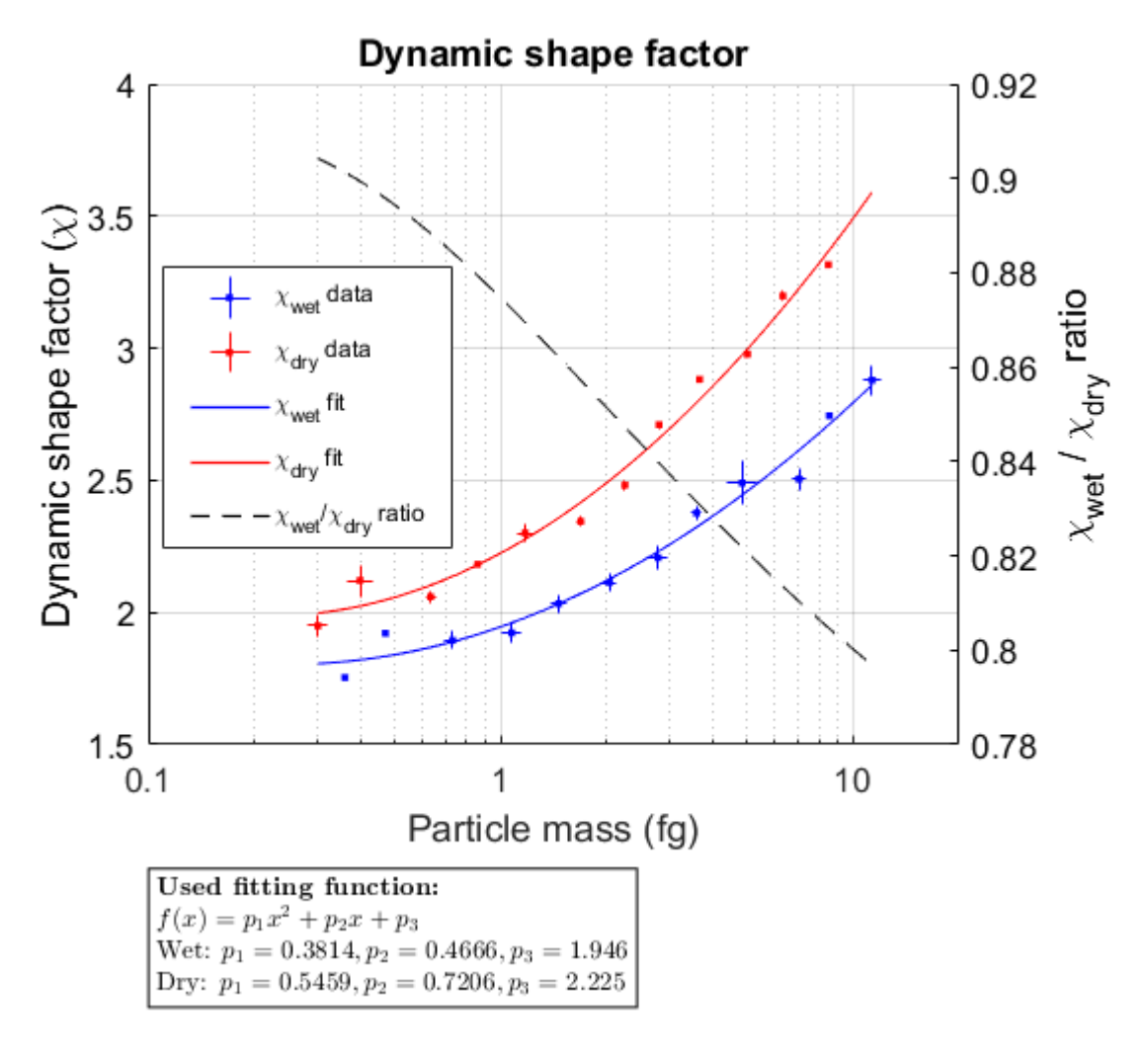


from the mass–mobility relationship $m_p \alpha d_m^{D_f}$ (Olfert et al., 2007; Schmidt-Ott et al., 1990; Skillas et al., 1998) using a least-squares fit with a power-law relationship. The approach is equivalent to the formulation by DeCarlo et al. (2004), which relates the volume-equivalent diameter to mobility diameter through $d_{ve}^3 \alpha d_m^{D_f}$. Dry particles consistently exhibited higher χ values compared to wet particles, but the difference remained modest. This implies that while restructuring reduces porosity and increases compactness, residual morphological irregularities remain even after humidification and drying. One contributing factor is the inherently hydrophobic nature of soot, which limits the extent of restructuring during humidification (Mikhailov et al., 2006). The χ_{wet}/χ_{dry} ratio indicates that the difference in wet and dry particle morphology, however, grows stronger with increasing particle size. Together with effective density measurements, these findings confirm that humidity-driven restructuring systematically alters soot morphology, with more pronounced relative effects in the larger particle sizes.





230



220 Figure 3. Dynamic shape factors (χ) of wet and dry soot particles as a function of particle mass, together with the ratio χwed/χdry. For data fitting, particle mass was mapped to log10 space prior to fitting a quadratic polynomial separately for wet and dry conditions.

3.2 Particle size-resolved absorption cross-sections and their ratios.

Measurements for the size-resolved per-particle light absorption are shown in Figure 4. The three different panels correspond to the different CEPAS wavelengths, each showing the measured wet and dry per-particle absorption cross-sections with standard deviations, their fitted curves and the wet-to-dry absorption ratio. The shaded background around the dashed black line represents the propagated standard deviation of the ratio, calculated as described in Section 2.3.

The wet-to-dry absorption ratios show a decreasing trend across all wavelengths: from 1.38 to 0.76 in the blue, from 1.29 to 0.88 in the green, and from 1.21 to 1.00 in the red. The red channel exhibits the flattest profile, reaching a ratio of \sim 1 at \sim 1.6 fg and remaining near unity at larger particle masses. Interestingly, the ratios for all wavelengths cross below 1 in the 1–2 fg



1.8

1.6

1.4

1.2

8.0

0.6

10



mass range, which corresponds to a volume-equivalent diameter of $\sim 102-129$ nm for spheres at a soot density of 1.8 g cm⁻³. It is also notable that the propagated errors are substantial, indicating that the ratios carry a relatively high degree of uncertainty.

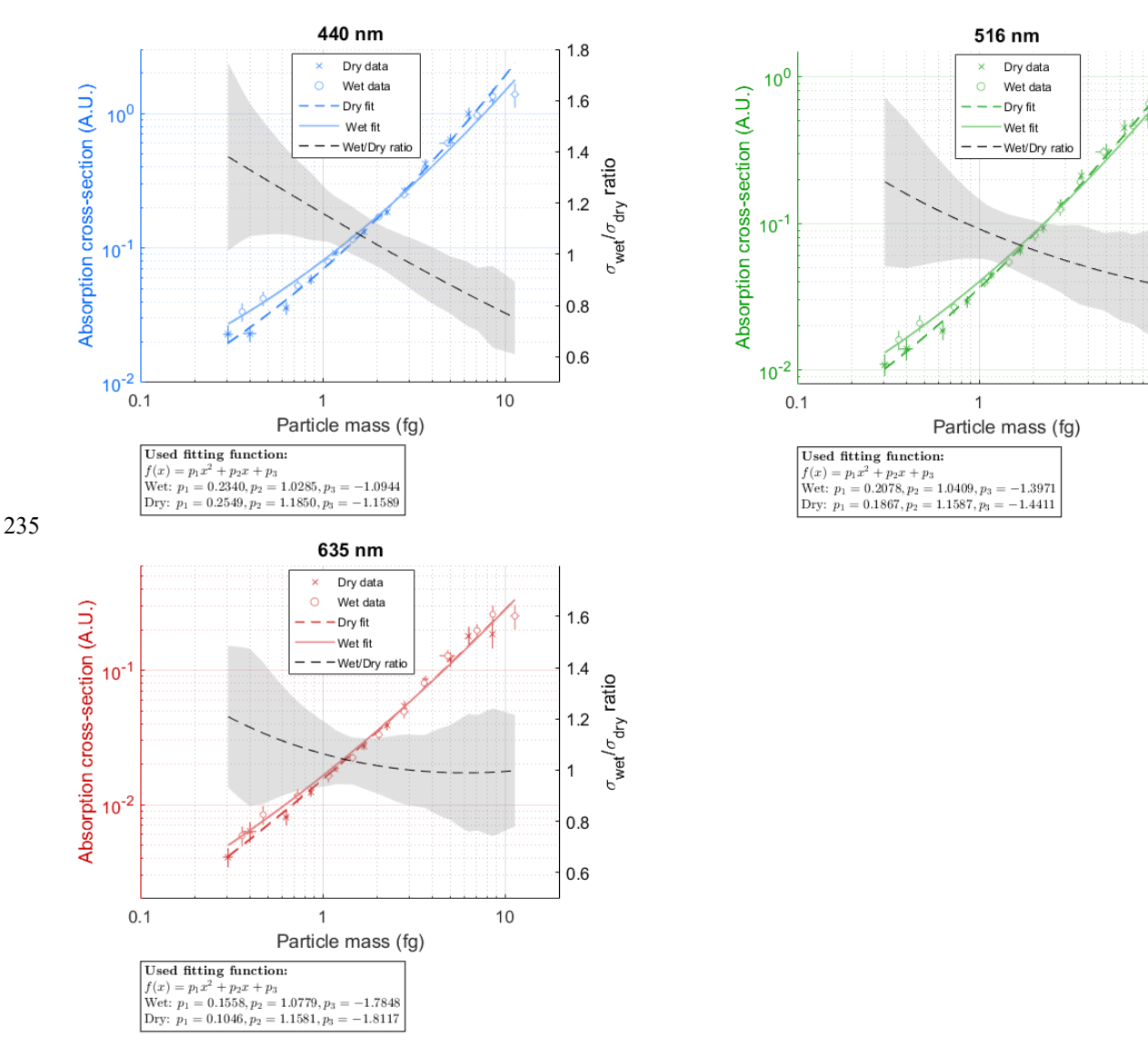


Figure 4. Per-particle light absorption cross-sections (σ) of wet and dry soot particles at three wavelengths (440, 516, and 635 nm) as a function of particle mass, together with the wet-to-dry absorption ratio ($\sigma_{wet}/\sigma_{dry}$). The black shaded background corresponds to the propagated standard deviation of the ratio. For data fitting, both particle mass and absorption cross-sections were mapped to log10 space prior to fitting a quadratic polynomial; the fitted curves were then exponentiated to obtain values on the original linear scale.



245

250

255

260

265

270

275



The observed decrease in the wet-to-dry absorption ratio from values above unity to below unity suggests a complex relationship between light absorption and particle morphology. For the smallest particles, the humidification—drying cycle, i.e. compaction, appears to enhance absorption, whereas for larger particles the effect reverses, despite the compaction process being stronger at higher masses in relative terms. This is evidenced by the effective density and dynamic shape factor data. The reversal likely results from multiple competing effects. One intuitive explanation is that more compact particles are effectively "darker", in the sense that they contain fewer voids and force light to traverse more bulk material. At the same time, compaction reduces the physical size of the particle, thereby reducing its projected cross-sectional area available for absorbing light. In this interpretation, the increase in cross-sectional area of more open (dry) aggregates eventually outweighs the enhanced "darkness" of compacted particles, leading to the observed decline in the wet-to-dry absorption ratio at higher particle masses.

A similar interpretation has been proposed by Liu et al. (2008), although their results are not directly comparable to those presented here, as their study modelled the absorption cross-section as a function of the fractal dimension rather than particle mass. In their framework, the term "darkness" used above corresponds to the increasing electromagnetic interaction among monomers as the aggregate becomes more compact. A more detailed theoretical description to this is provided by Liu et al. (2013) and Mulholland et al. (1994), who explain that, for small aggregates, dipole–dipole coupling among adjacent monomers enhances the local exciting field, which consequently increases absorption. These dipole–dipole coupling effects can also be understood as near-field interactions or multiple scattering within the aggregate. Although this enhancement of absorption for small compact aggregates is consistent with the present findings, Liu et al. (2013) also discussed the so-called shielding effect, whereby the outer monomers of a compact aggregate block light from reaching the inner monomers and hence reduce overall absorption. If assumed that more compact aggregates exhibit greater shielding efficiency at larger sizes, this interpretation would also explain the observed behavior in this study. While this specific detail was not fully addressed in Liu et al. (2013), similar considerations appear in the works of Dong et al. (2015), Luo et al. (2018), and Romshoo et al. (2021), all of whom discuss the interplay of coupling and shielding effects and report broadly consistent trends.

There are, however, studies presenting partially conflicting conclusions. Modelling by Kahnert and Devasthale (2011) and Scarnato et al. (2013) suggests that more open, fractal aggregates can exhibit higher absorption cross-sections than compact ones for a given volume-equivalent size, and that this tendency holds even for smaller aggregates. Experimental results are likewise mixed. For instance, Forestieri et al. (2018) and Radney et al. (2014) reported that the mass absorption cross-section of soot was largely independent of particle collapse, implying that absorption may be insensitive to changes in particle morphology. In contrast, other experimental work, such as Corbin et al. (2022) and references therein, observed measurable morphology-dependent variations in soot absorption. Among studies focusing on coated soot, many have reported absorption enhancement factors near unity for uncoated particles (e.g. Liu et al., 2017; Peng et al., 2016; Wu et al., 2018). While such results could be interpreted as evidence for size- and morphology-independence, the optical and structural properties of bare soot were not the primary focus in those works and thus remain less constrained experimentally.



280

285

290

300

305



In addition to these more conventional modelling studies, another branch of research has investigated the effects of minor structural features—that is, deviations from idealized point-contact aggregates—on soot optical properties. These features include heterogeneity in monomer size, surface roughness/irregularity, necking, and overlap. Of these, necking and overlap have received the most attention, as they directly affect the connectivity and local packing of monomers and can therefore be regarded as expressions of particle compactness. In idealized models, spherical and identical monomers are typically assumed to be in point contact with one another, whereas transmission electron microscopy images of real soot often show irregularities and partially fused or overlapping primary spheres (e.g. Moallemi et al., 2019). For a detailed discussion of the parameterization of necking and overlap, the reader is referred to Bescond et al. (2013, 2014) and Brasil et al. (1999).

Similarly to studies presented above, the results of those investigating the effects of necking and overlap are mixed: increased aggregate compactness may result in either increase or decrease in absorption depending on several different factors. Yon et al. (2015) reported that necking and overlap significantly decreased absorption at near UV but slightly or moderately increased it at longer wavelengths. Likewise, Doner et al. (2017) reported an increase in absorption at wavelengths in the visible and near-infrared regions. Skorupski and Mroczka (2014) found that the effect of overlap peaks at a certain degree of contact ($Cow \approx 0.18$) and then decreases; the peak position depends on the aggregate's total volume and refractive index, suggesting that electromagnetic resonances within the inter-monomer gaps play an important role. Variations in the refractive index were shown to shift the position of this peak, which they attributed to wavelength-dependent field enhancement near the contact regions. In contrast, Teng et al. (2019) concluded that the optical effects of such structural variations are primarily linked to their influence on total aggregate volume or mass, leading to only modest ($\sim 5\%$) changes in mass-specific optical properties.

295 4 Summary and conclusions

This study experimentally investigated the effects of morphological transformation on the light absorption properties of soot. Fresh soot particles were generated using an inverted-flame burner and subsequently compacted through a controlled wet–dry cycling procedure. Absorption measurements were performed at three wavelengths using a Cantilever-Enhanced Photoacoustic Spectrometer (CEPAS) coupled with a Differential Mobility Analyzer (DMA) and a Centrifugal Particle Mass Analyzer (CPMA). The combined setup enabled determination of the particle effective density, dynamic shape factor, and mass-resolved absorption cross-sections. Although primarily designed as a laboratory-based proof-of-concept, the study provides quantitative insight into how soot morphology and particle size jointly influence absorption efficiency.

The results showed that for small particles the absorption cross-section increased after humidification—drying but decreased for larger particles, with the wet-to-dry absorption ratio transitioning from values above unity to below unity across the particle mass range. This crossover behavior suggests a complex interplay between soot compactness and optical response. The findings are consistent with the theoretical framework in which absorption is governed by two competing effects: dipole—dipole coupling and optical shielding. At moderate compaction, reduced inter-monomer spacing enhances near-field

https://doi.org/10.5194/ar-2025-38 Preprint. Discussion started: 24 November 2025

© Author(s) 2025. CC BY 4.0 License.



310

315

325

330



electromagnetic coupling, increasing the local field strength and, consequently, the absorption cross-section. At higher compaction and increased physical size, however, outer monomers increasingly screen the interior of the aggregate from

incident radiation, leading to reduced absorption despite the stronger structural collapse. The results of this study thus

experimentally capture this transition between coupling-dominated and shielding-dominated regimes, which has been

predicted by earlier modeling studies (e.g., Liu et al., 2008; Mulholland et al., 1994; Dong et al., 2015; Luo et al., 2018).

Despite these consistencies, soot optical behavior remains an area of ongoing debate. Some previous experimental and

numerical studies have reported minimal or no dependence of absorption on aggregate morphology, or higher absorption for more open (fractal) structures even at smaller aggregate sizes (e.g., Kahnert and Devasthale, 2011; Scarnato et al., 2013;

Forestieri et al., 2018). Such discrepancies likely arise from differences in particle generation methods, degrees of

compaction, coating state, and the treatment of minor structural features such as monomer necking and overlap, which can

influence the optical coupling strength. These variations highlight the need for standardized experimental approaches and

controlled morphology-only studies to isolate the contribution of structure from that of composition.

A key limitation of the present work was the relatively weak morphological collapse of the soot aggregates, which was likely influenced by their inherent hydrophobicity. The inverted-flame burner used in this study operates on clean gaseous fuels,

producing nearly pure elemental carbon with minimal surface functional groups or condensed organics. Such "bare" soot is

highly hydrophobic and thus resists restructuring during humidification-drying cycles. In contrast, soot containing more

oxidized or organic components tends to collapse more readily. A stronger restructuring—potentially achievable through the

introduction of organic coatings or partially oxidized soot—might have amplified the observed differences in absorption.

Additional sources of uncertainty include the assumption of constant particle mass throughout the humidification-drying

process.

Overall, the findings demonstrate that morphological transformation alone can alter soot absorption in a non-monotonic

manner, with enhancement for smaller aggregates and suppression for larger, more compact ones. This highlights the

importance of particle morphology as an independent variable in soot optical modeling and climate-relevant radiative forcing

assessments. Future work should aim to extend these observations across a broader range of soot types and humidification

conditions, and to combine controlled laboratory experiments with numerical modeling to develop a more unified

understanding of soot light absorption.

Data availability

335 All measurement data are available on Zenodo: https://doi.org/10.5281/zenodo.17379625. For more details, contact Joel

Kuula (joel.kuula@helsinki.fi or joel.kuula@fmi.fi).





Author contributions

J.Ku.: Conceptualization, Methodology, Investigation, Formal analysis, Writing – original draft, Funding acquisition; J.Ka.:
 Methodology, Writing – review & editing; T.M.: Methodology, Writing – review & editing; A.V.: Formal analysis, Writing
 – review & editing; H.T.: Writing – review & editing, Resources, Funding acquisition; T.H.: Writing – review & editing, Funding acquisition; M.V.: Writing – review & editing, Resources, Funding acquisition.

Competing interests

At least one of the (co-)authors is a member of the editorial board of Aerosol Research. Dr. Tuomas Hieta is employed by Gasera Ltd., the company that manufactures the photoacoustic cell used in the CEPAS. The authors have no other competing interests to declare.

Financial support

This work was supported by the Academy of Finland under grant 349544 and by the Jane and Aatos Erkko Foundation for the project "Compact and precise sensor for global black carbon monitoring".

Acknowledgements

350 This manuscript was proofread and language-edited using AI tools.

References

Adachi, K., Chung, S. H. and Buseck, P. R.: Shapes of soot aerosol particles and implications for their effects on climate, J. Geophys. Res. Atmos., 115(15), 1–9, doi:10.1029/2009JD012868, 2010.

Bescond, A., Yon, jérôme, Girasole, T., Jouen, C., Rozé, C. and Coppalle, A.: Numerical investigation of the possibility to determine the primary particle size of fractal aggregates by measuring light depolarization, J. Quant. Spectrosc. Radiat. Transf., 126, 130–139, doi:10.1016/j.jqsrt.2012.10.011, 2013.

Bescond, A., Yon, J., Ouf, F. X., Ferry, D., Delhaye, D., Gaffié, D., Coppalle, A. and Rozé, C.: Automated determination of aggregate primary particle size distribution by tem image analysis: Application to soot, Aerosol Sci. Technol., 48(8), 831–841, doi:10.1080/02786826.2014.932896, 2014.

Bischof, O. F., Weber, P., Bundke, U., Petzold, A. and Kiendler-Scharr, A.: Characterization of the Miniaturized Inverted Flame Burner as a Combustion Source to Generate a Nanoparticle Calibration Aerosol, Emiss. Control Sci. Technol., 6(1), 37–46, doi:10.1007/s40825-019-00147-w, 2020.





- Bond, T. C. and Bergstrom, R. W.: Light absorption by carbonaceous particles: An investigative review, Aerosol Sci. Technol., 40(1), 27–67, doi:10.1080/02786820500421521, 2006.
- 365 Brasil, A. M., Farias, T. L. and Carvalho, M. G.: A recipe for image characterization of fractal-like aggregates, J. Aerosol Sci., 30(10), 1379–1389, doi:10.1016/S0021-8502(99)00026-9, 1999.
 - Cappa, C. D., Onasch, T. B., Massoli, P., Worsnop, D. R., Bates, T. S., Cross, E. S., Davidovits, P., Hakala, J., Hayden, K. L., Jobson, B. T., Kolesar, K. R., Lack, D. A., Lerner, B. M., Li, S. M., Mellon, D., Nuaaman, I., Olfert, J. S., Petäjä, T., Quinn, P. K., Song, C., Subramanian, R., Williams, E. J. and Zaveri, R. A.: Radiative absorption enhancements due to the
 - mixing state of atmospheric black carbon, Science (80-.)., 337(6098), 1078-1081, doi:10.1126/science.1223447, 2012. Cappa, C. D., Zhang, X., Russell, L. M., Collier, S., Lee, A. K. Y., Chen, C. L., Betha, R., Chen, S., Liu, J., Price, D. J., Sanchez, K. J., McMeeking, G. R., Williams, L. R., Onasch, T. B., Worsnop, D. R., Abbatt, J. P. D. and Zhang, Q.: Light Absorption by Ambient Black and Brown Carbon and its Dependence on Black Carbon Coating State for Two California, USA, Cities in Winter and Summer, J. Geophys. Res. Atmos., 124(3), 1550–1577, doi:10.1029/2018JD029501, 2019.
- China, S., Mazzoleni, C., Gorkowski, K., Aiken, A. C. and Dubey, M. K.: Morphology and mixing state of individual freshly 375 emitted wildfire carbonaceous particles, Nat. Commun., 4, 1–7, doi:10.1038/ncomms3122, 2013. China, S., Scarnato, B., Owen, R. C., Zhang, B., Ampadu, M. T., Kumar, S., Dzepina, K., Dziobak, M. P., Fialho, P., Perlinger, J. A., Hueber, J., Helmig, D., Mazzoleni, L. R. and Mazzoleni, C.: Morphology and mixing state of aged soot particles at a remote marine free troposphere site: Implications for optical properties, Geophys. Res. Lett., 42(4), 1243–1250, 380 doi:10.1002/2014GL062404, 2015.
 - Corbin, J. C., Johnson, T. J., Liu, F., Sipkens, T. A., Johnson, M. P., Lobo, P. and Smallwood, G. J.: Size-dependent mass absorption cross-section of soot particles various Carbon N. Y., 192. from sources, 438-451, doi:10.1016/j.carbon.2022.02.037, 2022.
- Davies, C. N.: Definitive equations for the fluid resistance of spheres, Proc. Phys. Soc., 57(4), 259-270, doi:10.1088/0959-5309/57/4/301, 1945. 385
 - DeCarlo, P. F., Slowik, J. G., Worsnop, D. R., Davidovits, P. and Jimenez, J. L.: Particle morphology and density characterization by combined mobility and aerodynamic diameter measurements. Part 1: Theory, Aerosol Sci. Technol., 38(12), 1185–1205, doi:10.1080/027868290903907, 2004.
- Doner, N., Liu, F. and Yon, J.: Impact of necking and overlapping on radiative properties of coated soot aggregates, Aerosol 390 Sci. Technol., 51(4), 532–542, doi:10.1080/02786826.2016.1275513, 2017.
- Dong, J., Zhao, J. M. and Liu, L. H.: Morphological effects on the radiative properties of soot aerosols in different internally mixing states with sulfate, J. Quant. Spectrosc. Radiat. Transf., 165, 43-55, doi:10.1016/j.jqsrt.2015.06.025, 2015.
 - Forestieri, S. D., Helgestad, T. M., Lambe, A. T., Renbaum-Wolff, L., Lack, D. A., Massoli, P., Cross, E. S., Dubey, M. K., Mazzoleni, C., Olfert, J. S., Sedlacek, A. J., Freedman, A., Davidovits, P., Onasch, T. B. and Cappa, C. D.: Measurement
- 395 and modeling of the multiwavelength optical properties of uncoated flame-generated soot, Atmos. Chem. Phys., 18(16), 12141–12159, doi:10.5194/acp-18-12141-2018, 2018.





- Fuller, K. A.: Scattering and absorption cross sections of compounded spheres II Calculations for external aggregation, J. Opt. Soc. Am. A, 12(5), 881, doi:10.1364/JOSAA.12.000881, 1995.
- Kahnert, M. and Devasthale, A.: Black carbon fractal morphology and short-wave radiative impact: A modelling study, 400 Atmos. Chem. Phys., 11(22), 11745–11759, doi:10.5194/acp-11-11745-2011, 2011.
 - Kahnert, M. and Kanngießer, F.: Modelling optical properties of atmospheric black carbon aerosols, J. Quant. Spectrosc. Radiat. Transf., 244, 106849, doi:10.1016/j.jqsrt.2020.106849, 2020.
 - Karhu, J., Kuula, J., Virkkula, A., Timonen, H., Vainio, M. and Hieta, T.: Cantilever-enhanced photoacoustic measurement of light-absorbing aerosols, Aerosol Sci. Technol., 56(1), 92–100, doi:10.1080/02786826.2021.1998338, 2021.
- Karhu, J., Mikkonen, T., Kuula, J., Virkkula, A., Ikonen, E., Vainio, M., Timonen, H. and Hieta, T.: Field-deployable cantilever-enhanced photoacoustic instrument for aerosol light absorption measurement at three wavelengths, Aerosol Res., 3(1), 113–124, doi:10.5194/ar-3-113-2025, 2025.
 - Kazemimanesh, M., Moallemi, A., Thomson, K., Smallwood, G., Lobo, P. and Olfert, J. S.: A novel miniature inverted-flame burner for the generation of soot nanoparticles, Aerosol Sci. Technol., 53(2), 184–195,
- 410 doi:10.1080/02786826.2018.1556774, 2019.
 - Khalizov, A. F., Xue, H., Wang, L., Zheng, J. and Zhang, R.: Enhanced Light Absorption and Scattering by Carbon Soot Aerosol Internally Mixed with Sulfuric Acid, J. Phys. Chem. A, 113(6), 1066–1074, doi:10.1021/jp807531n, 2009.
 - Kuula, J., Karhu, J., Mikkonen, T., Grahn, P., Virkkula, A., Timonen, H., Hieta, T. and Vainio, M.: Validation of cantilever-enhanced photoacoustic particle-size-resolved light absorption measurement using nigrosin reference particles and Mie modelling, Aerosol Res., 3(1), 1–13, doi:10.5194/ar-3-1-2025, 2025.
 - Lack, D. A., Massoli, P., Lack, D. A., Massoli, P., Cappa, C. D., Cross, E. S., Ahern, A. T., Davidovits, P., Onasch, T. B., Davidovits, P. and Onasch, T. B.: Absorption enhancement of coated absorbing aerosols: Validation of the photo-acoustic technique for measuring the enhancement, Aerosol Sci. Technol., 43(10), 1006–1012, doi:10.1080/02786820903117932, 2009.
- Leskinen, J., Hartikainen, A., Väätäinen, S., Ihalainen, M., Virkkula, A., Mesceriakovas, A., Tiitta, P., Miettinen, M., Lamberg, H., Czech, H., Yli-Pirilä, P., Tissari, J., Jakobi, G., Zimmermann, R. and Sippula, O.: Photochemical Aging Induces Changes in the Effective Densities, Morphologies, and Optical Properties of Combustion Aerosol Particles, Environ. Sci. Technol., 57(13), 5137–5148, doi:10.1021/acs.est.2c04151, 2023.
- Leys, C., Ley, C., Klein, O., Bernard, P. and Licata, L.: Detecting outliers: Do not use standard deviation around the mean, use absolute deviation around the median, J. Exp. Soc. Psychol., 49(4), 764–766, doi:10.1016/j.jesp.2013.03.013, 2013.
- Liu, D., Whitehead, J., Alfarra, M. R., Reyes-Villegas, E., Spracklen, D. V., Reddington, C. L., Kong, S., Williams, P. I., Ting, Y. C., Haslett, S., Taylor, J. W., Flynn, M. J., Morgan, W. T., McFiggans, G., Coe, H. and Allan, J. D.: Black-carbon absorption enhancement in the atmosphere determined by particle mixing state, Nat. Geosci., 10(3), 184–188, doi:10.1038/ngeo2901, 2017.





- 430 Liu, F., Wong, C., Snelling, D. R. and Smallwood, G. J.: Investigation of absorption and scattering properties of soot aggregates of different fractal dimension at 532 nm Using RDG and GMM, Aerosol Sci. Technol., 47(12), 1393–1405, doi:10.1080/02786826.2013.847525, 2013.
 - Liu, L., Mishchenko, M. I. and Patrick Arnott, W.: A study of radiative properties of fractal soot aggregates using the superposition T-matrix method, J. Quant. Spectrosc. Radiat. Transf., 109(15), 2656–2663, doi:10.1016/j.jqsrt.2008.05.001,
- 435 2008.
 Liu, S., Aiken, A. C., Gorkowski, K., Dubey, M. K., Cappa,
 - Liu, S., Aiken, A. C., Gorkowski, K., Dubey, M. K., Cappa, C. D., Williams, L. R., Herndon, S. C., Massoli, P., Fortner, E. C., Chhabra, P. S., Brooks, W. A., Onasch, T. B., Jayne, J. T., Worsnop, D. R., China, S., Sharma, N., Mazzoleni, C., Xu, L., Ng, N. L., Liu, D., Allan, J. D., Lee, J. D., Fleming, Z. L., Mohr, C., Zotter, P., Szidat, S. and Prévôt, A. S. H.: Enhanced light absorption by mixed source black and brown carbon particles in UK winter, Nat. Commun., 6, doi:10.1038/ncomms9435, 2015.
 - Luo, J., Zhang, Y., Zhang, Q., Wang, F., Liu, J. and Wang, J.: Sensitivity analysis of morphology on radiative properties of soot aerosols, Opt. Express, 26(10), A420, doi:10.1364/oe.26.00a420, 2018.
 - Matsui, H., Hamilton, D. S. and Mahowald, N. M.: Black carbon radiative effects highly sensitive to emitted particle size when resolving mixing-state diversity, Nat. Commun., 9(1), 1–11, doi:10.1038/s41467-018-05635-1, 2018.
 - 445 Michelsen, H. A.: Probing soot formation, chemical and physical evolution, and oxidation: A review of in situ diagnostic techniques and needs., 2017.
 - Mikhailov, E. F., Vlasenko, S. S., Podgorny, I. A., Ramanathan, V. and Corrigan, C. E.: Optical properties of soot-water drop agglomerates: An experimental study, J. Geophys. Res. Atmos., 111(7), 1–16, doi:10.1029/2005JD006389, 2006.
 - Moallemi, A., Kazemimanesh, M., Corbin, J. C., Thomson, K., Smallwood, G., Olfert, J. S. and Lobo, P.: Characterization of black carbon particles generated by a propane-fueled miniature inverted soot generator, J. Aerosol Sci., 135(May), 46–57, doi:10.1016/j.jaerosci.2019.05.004, 2019.
 - Mulholland, G. W., Bohren, C. F. and Fuller, K. A.: Light Scattering by Agglomerates: Coupled Electric and Magnetic Dipole Method, Langmuir, 10(8), 2533–2546, doi:10.1021/la00020a009, 1994.
 - Olfert, J. S., Symonds, J. P. R. and Collings, N.: The effective density and fractal dimension of particles emitted from a light-duty diesel vehicle with a diesel oxidation catalyst, J. Aerosol Sci., 38(1), 69–82, doi:10.1016/j.jaerosci.2006.10.002, 2007.
 - Pagels, J., Khalizov, A. F., McMurry, P. H. and Zhang, R. Y.: Processing of soot by controlled sulphuric acid and water condensation mass and mobility relationship, Aerosol Sci. Technol., 43(7), 629–640, doi:10.1080/02786820902810685, 2009.
 - Peng, J., Hu, M., Guo, S., Du, Z., Zheng, J., Shang, D., Zamora, M. L., Zeng, L., Shao, M., Wu, Y. S., Zheng, J., Wang, Y., Glen, C. R., Collins, D. R., Molina, M. J. and Zhang, R.: Markedly enhanced absorption and direct radiative forcing of black carbon under polluted urban environments, Proc. Natl. Acad. Sci. U. S. A., 113(16), 4266–4271, doi:10.1073/pnas.1602310113, 2016.





- Radney, J. G., You, R., Ma, X., Conny, J. M., Zachariah, M. R., Hodges, J. T. and Zangmeister, C. D.: Dependence of soot optical properties on particle morphology: Measurements and model comparisons, Environ. Sci. Technol., 48(6), 3169–3176, doi:10.1021/es4041804, 2014.
- Romshoo, B., Müller, T., Pfeifer, S., Saturno, J., Nowak, A., Ciupek, K., Quincey, P. and Wiedensohler, A.: Optical properties of coated black carbon aggregates: Numerical simulations, radiative forcing estimates, and size-resolved parameterization scheme, Atmos. Chem. Phys., 21(17), 12989–13010, doi:10.5194/acp-21-12989-2021, 2021.
- Scarnato, B. V., Vahidinia, S., Richard, D. T. and Kirchstetter, T. W.: Effects of internal mixing and aggregate morphology on optical properties of black carbon using a discrete dipole approximation model, Atmos. Chem. Phys., 13(10), 5089–5101, doi:10.5194/acp-13-5089-2013, 2013.
 - Schmidt-Ott, A., Baltensperger, U., Gäggeler, H. W. and Jost, D. T.: Scaling behaviour of physical parameters describing agglomerates, J. Aerosol Sci., 21(6), 711–717, doi:10.1016/0021-8502(90)90037-X, 1990.
- Skillas, G., Künzel, S., Burtscher, H., Baltensperger, U. and Siegmann, K.: High fractal-like dimension of diesel soot agglomerates, J. Aerosol Sci., 29(4), 411–419, doi:10.1016/S0021-8502(97)00448-5, 1998.
 - Skorupski, K. and Mroczka, J.: Effect of the necking phenomenon on the optical properties of soot particles, J. Quant. Spectrosc. Radiat. Transf., 141, 40–48, doi:10.1016/j.jqsrt.2014.03.001, 2014.
 - Sorensen, C. M.: The mobility of fractal aggregates: A review, Aerosol Sci. Technol., 45(7), 765–779, doi:10.1080/02786826.2011.560909, 2011.
- Teng, S., Liu, C., Schnaiter, M., Chakrabarty, R. K. and Liu, F.: Accounting for the effects of nonideal minor structures on the optical properties of black carbon aerosols, Atmos. Chem. Phys., 19(5), 2917–2931, doi:10.5194/acp-19-2917-2019, 2019.
 - Wentzel, M., Gorzawski, H., Naumann, K. H., Saathoff, H. and Weinbruch, S.: Transmission electron microscopical and aerosol dynamical characterization of soot aerosols, J. Aerosol Sci., 34(10), 1347–1370, doi:10.1016/S0021-8502(03)00360-4, 2003.
 - Wu, Y., Cheng, T., Liu, D., Allan, J. D., Zheng, L. and Chen, H.: Light Absorption Enhancement of Black Carbon Aerosol Constrained by Particle Morphology, Environ. Sci. Technol., 52(12), 6912–6919, doi:10.1021/acs.est.8b00636, 2018.
 - Yon, J., Bescond, A. and Liu, F.: On the radiative properties of soot aggregates part 1: Necking and overlapping, J. Quant. Spectrosc. Radiat. Transf., 162, 197–206, doi:10.1016/j.jqsrt.2015.03.027, 2015.
- Zhang, R., Khalizov, A. F., Pagels, J., Zhang, D., Xue, H. and McMurry, P. H.: Variability in morphology, hygroscopicity, and optical properties of soot aerosols during atmospheric processing, Proc. Natl. Acad. Sci. U. S. A., 105(30), 10291–10296, doi:10.1073/pnas.0804860105, 2008.
 - Zhang, Y., Favez, O., Canonaco, F., Liu, D., Močnik, G., Amodeo, T., Sciare, J., Prévôt, A. S. H., Gros, V. and Albinet, A.: Evidence of major secondary organic aerosol contribution to lensing effect black carbon absorption enhancement, npj Clim.
- 495 Atmos. Sci., 1(1), 47, doi:10.1038/s41612-018-0056-2, 2018.